International Journal of Thermophysics, Vol. 14, No. 2, 1993

Premelting Transition in Uranium Dioxide

J. P. Hiernaut,[1] G. J. Hyland,[2] and C. Ronchi[1]

Received December 7, 1992

Thermal analysis of the cooling curves of small samples of $UO_{2\pm x}$—initially laser heated (in a high-pressure autoclave to inhibit evaporation) on a sub-second time scale to temperatures just below their melting points $[T_m(x)]$—reveals, in the case of nominally stoichiometric $UO_{2.00}$, a significant, λ-like, heat capacity $[C_p(T)]$ peak near 2670 K; the cooling curves of samples exposed to a reducing environment, on the other hand, exhibit *undercooling*, characteristic of a first-order phase transition, while under oxidizing conditions it is found that the premelting transition readily disappears. These findings confirm Bredig's original prediction of a premelting transition in this material, in common with that found in other (nonactinide) fluorites near $0.85T_m$. A simple model is presented in terms of which the observed behavior can be rationalized. The model is based on the hypothesis that the premelting transition is due to Frenkel disordering of the oxygen sublattice—a process which is rendered *cooperative* by *attractive* interactions between complementary Frenkel defects (oxygen interstitials and vacancies); these interactions are treated in a "mean-field" approximation. The quantitative degree of maximum disorder (realized just above the transition) is, on the other hand, controlled by *repulsive* interactions between *like* defects—the inclusion of which, solely through their effect on the configurational entropy, satisfactorily reproduces the values inferred from recent high-temperature neutron diffraction experiments. Assuming that the phase transition in stoichiometric $UO_{2.00}$ is of second order, the model predicts a divergent heat capacity, C_v, which approximates well to the experimental (λ-like) C_p peak. Crucial to reproducing the observed behavior *away* from stoichiometry is the introduction of a (linear) dependence of the nonconfigurational partial entropy of formation on the prevailing concentration of intrinsic Frenkel defects in $UO_{2\pm x}$; interestingly, it is found that the line of calculated (but unrealized) second-order transitions in UO_{2+x} intersects the U_4O_9 phase boundary near to where a high-temperature diffuse order–disorder transition has

[1] CEC Joint Research Center, European Institute for Transuranium Elements, Karlsruhe, Germany.

[2] Department of Physics, University of Warwick, Coventry, CV4 7AL, United Kingdom.

0195-928X/93/0300-0259$07.00/0

been observed in the oxygen superlattice, suggesting that the second-order, λ-transition in $UO_{2.00}$ is the stoichiometric counterpart of this transition in U_4O_9.

KEY WORDS: high temperatures; pulse heating; solid λ-transition; uranium dioxide.

1. INTRODUCTION

This paper presents some interesting new results obtained from experiments employing *subsecond* pulse heating of small spherical samples of UO_2 ($\sim$1 mm in diameter) in a high-pressure autoclave, using a Nd-YAG laser. The essential new feature is the discovery of a weak inflexion-point plateau near $0.85T_m$ in the cooling curve of nominally stoichiometric samples of UO_2, initially heated to just below their melting temperature, T_m. Most interestingly, it is found that the occurrence of the plateau is sensitively dependent on whether the buffer gas is oxidizing or reducing—*no* plateaux being found under *oxidizing* conditions, while in a *reducing* environment the plateau typically exhibits *undercooling*, characteristic of a first-order phase transition, the temperature of which is found to increase with increasing reduction of the sample. Thermal analysis of the cooling curve (with respect to time) yields the heat capacity, $C_p(T)$—the inflexion-point plateau of the nominally stoichiometric sample entailing a sharp C_p peak—the existence of which was first *qualitatively* inferred by Bredig [1] in 1969 from consideration of the best available enthalpy data [2] on approximately stoichiometric urania, $UO_{2.003\pm0.003}$. Although our peak is much more λ-like than that obtained from a subsequent refined numerical differentiation [3] of the same enthalpy data [2], it is, nevertheless, located at a temperature close to where recent high-temperature neutron diffraction experiments [4] indicate a significant increase in the concentration of anion (oxygen) Frenkel defects to a value which appears to saturate around 15%—a behavior similar to that found [5] in other nonactinide fluorite structured materials, near $0.8T_m$, as the so-called "fast ion" (or superionic) phase is rapidly, but *continuously*, established [6]; again, however, the associated $C_p(T)$ peak (which in these other materials is *directly* measurable using steady-state methods [7], in consequence of their much lower T_m, $\sim$1000 K) is much broader and weaker than that now found for UO_2.

After summarizing the details of the experimental setup in Section 2, a simple model, consistent with the new $C_p(T)$ results, is presented in Section 3, based on the assumption that oxygen Frenkel disorder is

the predominant underlying process; the paper concludes with a brief consideration in Section 4 of the implications of the new results on the phase diagram of $UO_{2\pm x}$.

2. EXPERIMENTAL PROCEDURE

2.1. System

The experimental technique is based on thermal analysis of the cooling curve of a laser-heated spherical sample of Urania, obtained using the apparatus shown in Fig. 1. The sample, suspended by a thin tungsten

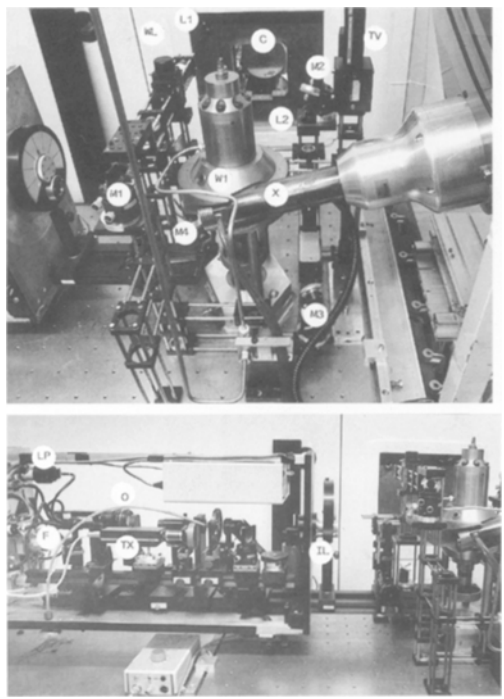

Fig. 1. Experimental system. Autoclave top view: M1, M2, M3, and M4, adjusting mirrors of the four laser beams; W1, laser window (W2, W3, and W4 are not visible); TV, sample monitoring television camera; L1 and L2, entries of the two main Nd–YAG laser beams and the He–He laser viewfinders; X, X-ray microfocus to measure sample dilation; C, high-speed X-ray camera; WL, protecting concrete wall. Side view: IL, intermediate lense for enlarging the sample image; O, pyrometer objective; F, fiber bundle for multichannel splitting; LP, He–He laser for pyrometer alignment; TX, television camera for monitoring the state of the measured surface.

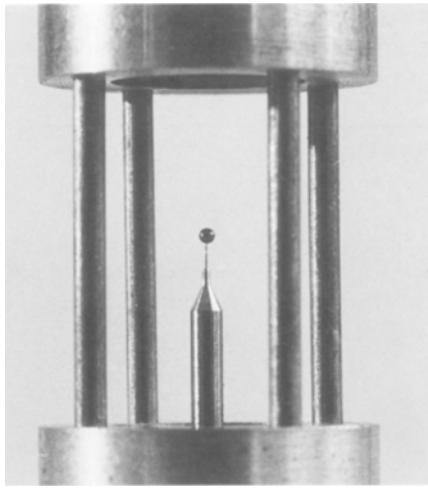

Fig. 2. Specimen mounting. The sphere of UO_2 has a diameter of approximately 1 mm. The support is a tungsten needle.

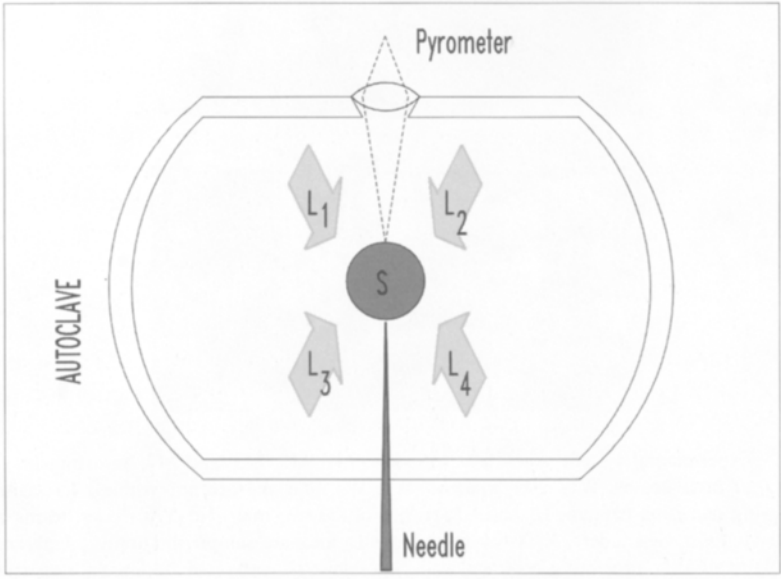

Fig. 3. Scheme of the specimen heating: L1, L2, L3, and L4 are equivalent, tetrahedrally oriented Nd–YAG laser beams.

needle (see Fig. 2), is positioned (see Fig. 3) in the center of an autoclave, at the point of convergence of four Nd-Yag laser beams of equal power, whose size is approximately equal to the sample diameter. The spatial power profiles of the beams are suitably tuned to obtain a sufficiently constant specific power deposition on the sample surface.

A videocamera (TV) provides a record of the sample image before, during, and after the short pulse, to check that no large sample displacements take place during heating, since these would adversely affect the temperature measurement.

Temperature is measured with a six-channel pyrometer positioned approximately 50 cm from the autoclave window, where a biconvex lens is mounted to provide an enlarged image of the measured area (a circular area of 150-μm size).

The detected wavelengths were 550, 650, 750, 850, 950, and 1000 nm, a complete measurement (including A/D conversion) being performed in less than 200 μs.

The signals were stored and subsequently analyzed in order to obtain the temperature and spectral emissivities of the sample. The precision of the temperature measurement was of the order of 0.5–1%. The method is described in detail elsewhere, [8].

2.2. Pulse Heating

The spherical sample, approximately 1 mm in diameter, was simultaneously heated by four tetrahedrally oriented Nd-YAG lasers. Temperatures of up to 3000 K were reached in less than 50 ms. The deposited power was adjusted to obtain a temperature plateau where the input power was balanced by the total losses (radiative, convective, and conductive). The plateau temperature was maintained for approximately 300 ms, after which the lasers were switched off. A computer code was used to calculate the heat propagation into the sample under realistic boundary conditions. The results of this analysis showed that at the end of the heating stage, the radial temperature gradient in the sample was less than $100\,\mathrm{K}\cdot\mathrm{mm}^{-1}$, except for a small zone (50 μm) surrounding the tungsten needle; detailed calculation of the global heat loss reveals, however, that this zone has a negligible effect on the overall thermal behavior of the sample.

The cooling rate of the sample was governed mainly by radiation heat loss and by heat convection in the autoclave gas, (different gases, He, Ar, and H_2, were used at pressures varying from 2 to 75 bar), as well as by the size of the sample.

The experimental cooling curve is normally smooth and sufficiently reproducible to enable the heat losses to be evaluated with a precision of

10–15%, if the heat capacity of the sample and its thermal conductivity are known. Vice versa, from a given cooling curve and heat loss, the heat capacity of the sample can be deduced [9].

2.3. Detection of Thermodynamical Transitions

Thermal analysis of laser pulse-heated samples has been used in our laboratory to investigate a variety of phase transitions. These are observed as perturbances of the cooling and/or heating rate with respect to the "regular" behavior, as calculated for a given setup and assumed material properties. In particular, if the transition is localized around a distinct temperature T_c, and the heat capacity of the sample is known at temperatures sufficiently far from T_c, then analysis of the extra contribution to C_p in the transition region is greatly faciliatated and is more accurate, for it depends only on the *ratio* of the measured cooling rate to the gradient dT/dt predicted in the *absence* of transition. This was the method adopted in our analysis of the premelting transition in UO_2.

2.4. The Sample

2.4.1. Before Treatment

The samples consist of 1-mm-diameter, effectively perfect, spheres of nominally stoichiometric UO_2 produced by a sol-gel method. To support the sample, a thin tungsten needle (see Fig. 2) was inserted into a 50-μm hole made using a high-power laser shot (of a few microseconds duration). A 10- to 50-μm thick layer around the hole was melted during this procedure, but the rest of the sample was not affected—either structurally or by the formation of cracks.

Two batches of material were available, the first (A) with high sintered density (95–97% theoretical density), and the second (B) with somewhat higher porosity (85–90% theoretical density).

2.4.2. After Treatment

The sample was pulse-heated up to maximum temperatures below the melting point. Ceramographs made after the treatment showed that the grain and pore structure was preserved (Figs. 4 and 5), confirming that melting had *not* occurred during the heating phase.

Shots were made in inert, reducing (inert gas + 3% hydrogen), and oxidizing (inert gas + 0.1-bar oxygen) atmospheres. In all the three cases, the sample did *not* show any second phase (metal or U_4O_9)—even after repeated pulses.

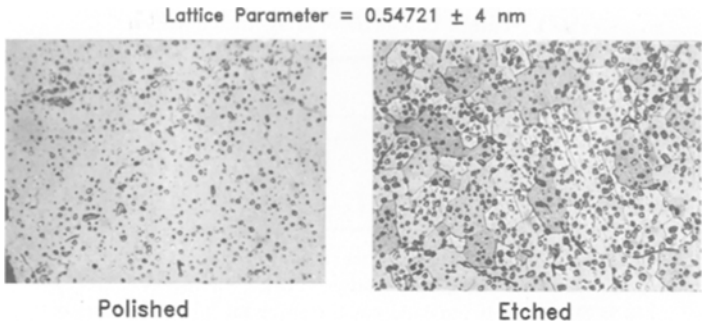

Fig. 4. Ceramograph of the samples heated in He:3% H_2. The lattice parameter (0.54721 nm) indicates a marked reduction of UO_2 during the shot. The sample does not show a metallic phase at magnifications up to 1000×.

X-ray analysis showed that the lattice parameter of samples treated in an inert atmosphere ranged between 0.54703 and 0.54709 nm; a further increase above these values was observed after repeated shots, indicating a progressive reduction from an initially slightly hyperstoichiometric sample. After treatment in hydrogen, a lattice parameter of 0.54721 nm was measured. This certainly corresponds to hypostoichiometric urania and, to our knowledge, is the highest lattice parameter of quenched f.c.c. UO_2 ever measured. Quenching of single-phase UO_{2-x} from high temperature is well-known to be extremely difficult due to the rapid precipitation of metallic uranium. Even in our case, it cannot be excluded that submicroscopic U-precipitates are formed. For this reason it is difficult to obtain a meaningful correlation between lattice parameter of quenched UO_{2-x} and stoichiometry. Furthermore, due to the small size of the samples,

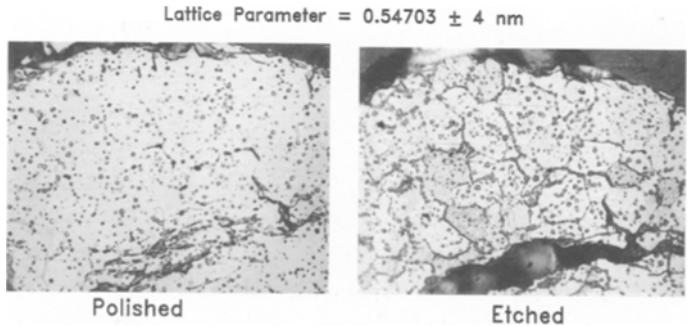

Fig. 5. The same as Fig. 4, after heating in 25-bar He. The lattice parameter (0.54703 nm) indicates an approximately stoichiometric composition.

Table I. Lattice Parameter of UO_2 After the Shots[a]

Atmosphere	Lattice parameter (nm)
IG: 0.1-bar oxygen	0.54697
Helium	0.54703
IG: 3% hydrogen	0.54721

[a] The parameter measured after a shot in inert gas (IG) + hydrogen is markedly larger than that of $UO_{2.00}$ (0.54707 − 0.54710 nm) and could well be the largest cell size of quenched f.c.c. uranium dioxide ever measured.

chemical analysis of O/U could not be performed with sufficient accuracy. Accordingly, the stoichiometries after the pulses could be only qualitatively assessed by reference to the measured lattice parameters (see Table I).

2.5. Results

The premelting transition was observed in samples heated to temperatures a few hundred degrees below the melting point of UO_2; the transition manifests itself as a weak inflexion-point plateau in the cooling curves. Meaningful thermal analysis can be performed if mean cooling rates of less than $10^4\,K \cdot s^{-1}$ are produced (Fig. 6). In the heat-up stage, the

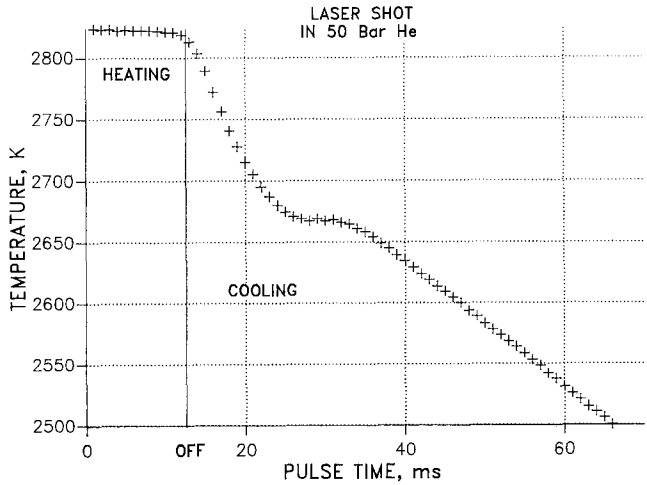

Fig. 6. Premelting transition in UO_2 as revealed by thermal analysis of a cooling sample, initially heated to 2850 K, for 300 ms, in 50-bar He.

temporal temperature gradient was larger by a factor of 10 and the transition could not, therefore, be so clearly identified.

With the samples in batch B (low sintered density) the transition was always observed, whereas in samples in batch A (high density) the transition was clearly observed only after a few shots at high temperature. In the

Table II. Summary of the Experimental Results Obtained for Different Pressures and Compositions of the Autoclave Gas[a]

Sample-shot-gas	T_{trans} (K)
1A-45-75 bar He	2615
1A-46-idem	2678
1A-47-idem	2617
1A-48-idem	2727
1A-49-idem	2721
2A-60-25 bar He	2648
2A-62-idem	2629
2A-64-idem	2614
2A-65-O_2 + He (molten)	
3A-70-2 bar Ar + 3% H_2	2850
3A-71-idem	2852
4A-73-25 bar He	2866
4A-74-idem	2880
4A-75-idem	2880
4A-77-idem	2835
5A-82-4 bar Ar + 3% H_2 (molten)	2940
5A-83-idem	
5A-84-idem	
5A-85-idem	
6A-94-50 bar He	2648
6A-95-idem	2668
6A-97-idem	2734
7A-100-4 bar Ar + 3% H_2	2755
7A-101-idem	
7A-102-idem	2847
7A-103-idem	2838
7A-104-idem	2918
7A-105-idem	2950
8B-114-40 bar He	2830
8B-116-idem	2840

[a] T_{trans} is the temperature at which the plateau occurs in the cooling curve of the identified samples, previously laser-heated to a temperature T_{max} ($< T_{melt}$).

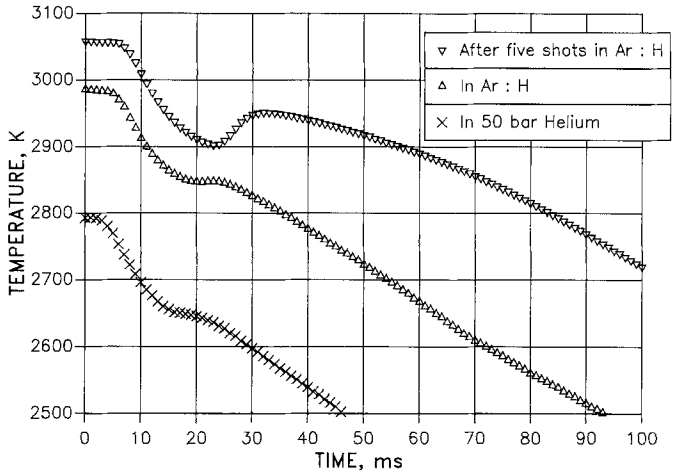

Fig. 7. Cooling curves of samples heated in different atmospheres. The curve at the top was displayed by a sample repeatedly heated in a reducing atmosphere; an undercooling effect is clearly visible in the "plateau" region.

light of the following results, this effect finds explanation in terms of the different evaporation conditions of the samples in the two structural configurations—the former (B) providing many more free surfaces than exist in batch A, where the porosity was essentially closed.

The transition temperature in *nominally stoichiometric* $UO_{2.00}$ lay in

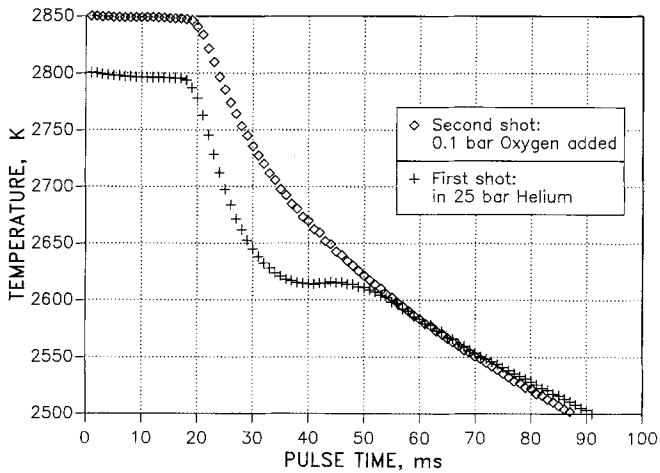

Fig. 8. Cooling curves of samples heated in inert and oxidizing atmosphere, respectively; in the latter case, the transition plateau disappears.

the interval $T_c = 2670 \pm 30$ K; see Table II, where the cited scatter is approximately twice the precision of the temperature measurement. This value of T_c is actually *coincident* with that proposed by Bredig [1] but is somewhat higher than that (2610 K) found in Ref. 3.

Interestingly, if a sample was initially heated above its melting point, no transition appeared, even in subsequent pulse heat treatments of the sample to submelting temperatures.

It was soon realized that the transition temperature showed a systematic tendency to increase if a sequence of pulses was applied to the *same* sample. The effect was first detected in an inert gas atmosphere and was found to be more pronounced at low pressures. To check whether this effect was reasonably ascribable to a reduction of the sample by vaporization, 3% hydrogen was introduced into the inert buffer gas in the autoclave. This led to a further increase in the transition temperature, which (after repeated shots) attained a value of 2950 K (Fig. 7). The lattice parameter of the sample showing the highest transition temperature was found to be much *larger* than that of stoichiometric $UO_{2.00}$, consistent with a marked reduction from the initial composition. Furthermore, it was observed that the transitions at higher temperatures exhibit undercooling effects,[3] typical of first-order phase transitions (see Fig. 7).

The experiment was then repeated by heating the sample in an oxidizing atmosphere (inert gas + 0.1-bar O_2). The results were even more dramatic—the inflexion-point plateau *disappearing* completely (Fig. 8), indicating either that the transition did *not* occur or that it is located *outside* of the explored temperature range (2300–3000 K).

The results of the various experiments are presented in Table II, which contains clear evidence that the premelting transition in $UO_{2\pm x}$ is strongly affected by stoichiometry—the transition temperature increasing with x in the hypostoichiometric oxide, while in the hyperstoichiometric oxide, *no* transition is detected [1].

The measured cooling curves have been analyzed with the above-mentioned method to obtain the extra contribution to C_p of the premelting transition. This extra contribution is calculated with respect to the experimental C_p baseline[4] plotted in Fig. 9. Figure 10 shows that the heat capacity peak is very localized around the transition temperature, where it effectively diverges to infinity.

[3] Undercooling is associated with a transition time delay due to the finite nucleation rate of the low-temperature phase.

[4] In this respect it is worth remarking that this baseline could contain contributions belonging to the "tails" of the C_p peak associated with the premelting transition; this should be borne in mind in the following theoretical treatment.

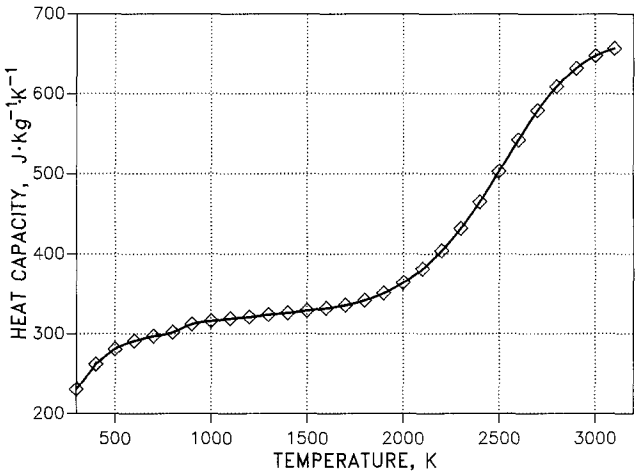

Fig. 9. Heat capacity of UO_2 as a function of temperature—used as a reference in the analysis of the experiments.

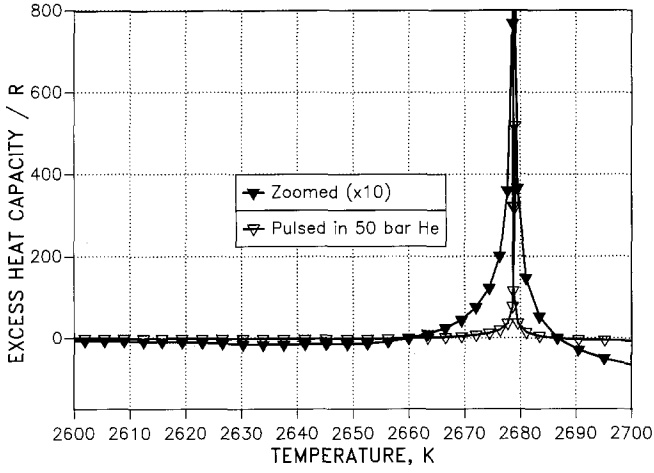

Fig. 10. Excess heat capacity (in units of the gas constant, R) due to the premelting transition (open triangles), as deduced from the cooling curve. The curve designated by filled triangles corresponds to a ordinate scale reduction by a factor 10.

3. THEORETICAL CONSIDERATIONS

We now present a simple model (which neglects the distinction between C_p and C_v) in terms of which the new $C_p(T)$ results can be understood—in particular, with respect to their stoichiometry dependence.

Consistent with the situation in the case of the *stoichiometric*, non-actinide fluorites (like $SrCl_2$), where the high-temperature ("fast ion") phase is established rapidly but *continuously* [as indicated, e.g., by the T dependence of their electrical conductivity (6)], we assume that the λ-like $C_p(T)$ peaks characteristic of the (nominally) *stoichiometric* UO_2 samples are associated with a *second-order* phase transition (the simplest, *continuous*, non-first-order possibility) involving oxygen Frenkel disorder, crucial to the occurrence of which is the existence of an attractive interaction between pairs of complementary defects (i.e., interstitials and vacancies), whereby the actual degree of disorder realized at a particular temperature depends on that already established, in such a way that it becomes progressively easier to produce more defects—i.e., the attractive interaction renders the process "cooperative." The quantitative degree of maximum disorder (realized just above the phase transition) is, on the other hand, limited by repulsive interactions between like defect species [10].

If the oxygen Frenkel disorder equilibrium is represented (in a obvious notation) as follows,

$$O_L + V_i^0 \rightleftharpoons V_L^0 + O_i \tag{1}$$

then at stoichiometry ($x = 0$), the concentrations of interstitials, $[O_i]$, and vacancies $[V_L^0]$ satisfy

$$[O_i] = [V_L^0] \qquad (\equiv n) \tag{2}$$

while, generally (i.e., for arbitrary x) the following constraint conditions hold, consistent with the fluorite structure of the material, in which the *total* concentration of oxygen lattice sites (normalized to the total number of U atoms per unit volume, N) is equal to *twice* that of the interstitial sites,

$$\begin{aligned} [O_L] + [V_L^0] &= 2 \\ [O_i] + [V_i^0] &= 1 \end{aligned} \tag{3}$$

The crucial *attractive* interactions between interstitials and vacancies is most simply treated within a "mean-field" approximation, in which the defect internal energy, U, is assumed to be dependent on the defect species

complementary to that which characterizes the *intrinsic* disorder in $UO_{2\pm x}$, according to

$$U_{UO_{2+x}} = wN_v - \frac{\lambda}{2N} N_v N_i; \qquad U_{UO_{2-x}} = wN_i - \frac{\lambda}{2N} N_i N_v \tag{4}$$

The energy λ (>0) parametrizes the admitted attractive interaction, and w is the energy required to create a single $O_i - V_L^0$ pair in the *absence* of any such interaction. Estimates of w can be obtained as *twice* the activation energy of the rise in $[O_i]$ in nominally stoichiometric UO_2—as indicated by the neutron scattering experiments [4]—*well below* the transition (i.e., at temperatures low enough to validate the neglect of defect interactions); alternatively, oxygen diffusion data on UO_{2+x} in the limit $x \to 0$ can be used [11]. λ, on the other hand, is a parameter *peculiar* to the adopted mean-field description of the attractive defect interactions and, as such, can be quantified only within the context of the model.

The inclusion of *repulsive* interactions between like defect species must, intuitively, be considered to entail a certain *non*occupancy of defect sites neighboring an already occupied site—e.g., that the occupation of an interstitial site by an oxygen atom effectively "blocks" the occupancy of a certain number of *neighboring* interstitial sites by *other* oxygens. Following Speiser and Spretnak [12], it is assumed that the effect of this blocking is manifest solely in the configurational entropy, S_{conf}, the expression of which still assumes the defects to be *randomly* distributed but over a *reduced* number of sites—the N interstitial sites being reduced by a factor α, and the $2N$ lattice sites by a factor β—i.e.,

$$S_{conf} = k \ln[{}^{\alpha N}C_{N_i} \cdot {}^{\beta 2N}C_{N_v}] \tag{5}$$

To determine the blocking factor α and β, we follow Hagemark and Broli's [13] treatment of α for UO_{2+x}, and adapt it to include the intrinsic Frenkel disorder under discussion, in both $UO_{2.00}$ and $UO_{2\pm x}$. We thus argue that (initially) each O_i blocks the occupancy of the 12 nearest-neighbor (nn) interstitial sites, while each V_L^0 blocks the occupancy of the six nn lattice sites. With increasing disorder, the average number of sites blocked per defect must decrease, since neighboring defects (of the same species) eventually block some of the same sites. Thus instead of one interstitial site being available per UO_2 formula unit, there is only a fraction α (<1) given by

$$\alpha = (1 - \alpha[O_i])^{12} \simeq 1 - 12\alpha[O_i] \tag{6}$$

$\alpha[O_i]$ approximately represents the probability of finding one interstitial site occupied by an oxygen atom and, at the *same time*, no other nn inter-

stitial site; $(1-\alpha[O_i])$ is then the probability of finding an interstitial site unoccupied. In the presence of blocking, an "available" interstitial site is defined as one surrounded by 12 unoccupied nn interstitial sites.

Solving Eq. (6) for α yields

$$\alpha = \frac{1}{1+12[O_i]} \tag{6a}$$

At the temperatures ($T < 1500°C$) considered by Hagemark and Broli, intrinsic Frenkel disorder is negligible, whence $[O_i] \to x$, and Eq. (6a) entails an upper-phase boundary at $x = 0.25$, consistent with the phase diagram of the material. Continued use of Eq. (6a) at higher temperatures, where the degree of Frenkel disorder is significant, then permits the blocking effect of the repulsive interactions between interstitials to be incorporated *without* the introduction of any additional parameters, both for UO_{2+x}, where $[O_i] = n + x$, and for UO_{2-x}, where $[O_i] = n$.

Detailed analysis of the high-temperature neutron diffraction data [4] suggests, however, that for every Frenkel interstitial, *two* other oxygen ions are displaced from their regular lattice sites to interstitial positions in unit cells adjacent to that occupied by the Frenkel interstitial. The existence of such defect "clusters" suggests that the blocking be extended to at least *next* nearest neighbors, whence the factor 12 in the above expression for α is to be increased to 18; this is assumed in what follows—i.e.,

$$\alpha = \frac{1}{1+18[O_i]} \tag{7}$$

In the absence of any empirical counter-indications, an identical treatment of vacancy blocking will be adopted, whence

$$\beta = \frac{1}{1+18[V_L^0]} \tag{8}$$

although it should be appreciated that here the numbers of nn and next nn are *interchanged* from those relevant in the case of interstitials.

In terms of U and S_c, the Helmholtz free energy, F, is given by

$$F = F_0 + U(w, \lambda) - T[S_{conf}(\alpha, \beta) + S_{nc}] \tag{9}$$

where F_0 refers to the defect-free crystal, and S_{nc} denotes entropy contributions of a *non*configurational nature—such as that arising, for example, from the change in vibrational frequencies entailed by the Frenkel disordering equilibrium [Eq. (1)].

For given values of w, λ, and S_{nc}, the *equilibrium* concentration, $\bar{n}(T)$, of *intrinsic* defects at temperature T is given by the solution of

$$\partial F/\partial n = 0 \tag{10}$$

where $n \equiv [V_L^0]$ ($[O_i]$) for UO_{2+x}, (UO_{2-x}); in taking this derivative it is essential, however, that the n dependence of α and β be *neglected* [14].

In terms of $\bar{n}(T)$, the defect contribution to the heat capacity, $C_v(T)$, is given, via Eq. (4), by

$$C_v(T)\left(=\frac{\partial U}{\partial T}\right) = (w - \lambda\bar{n}(T))\frac{d\bar{n}}{dT} \tag{11}$$

Detailed investigation indicates that the observed trend of the transition temperature with x in UO_{2-x} can be correctly reproduced if a dependence of the nonconfigurational partial entropy, $\partial S_{nc}/\partial n$ ($\equiv \Delta S_{nc}$) on the defect concentration, n, of the following form is admitted:

$$\Delta S_{nc} \to \Delta S_{nc}^{-} = \Delta S_0^{-} + \mu^{-} n \tag{12}$$

Such a dependence is naturally entailed by the above *vibrational* identification of S_{nc}, since ΔS_{nc} then takes the following form [15]:

$$\Delta S_{nc} = k \ln\left[\left(\frac{\nu_L}{\nu_i}\right)\left(\frac{\nu_L}{\nu_L^i}\right)^{n^i}\left(\frac{\nu_L}{\nu_L^v}\right)^{n^v}\right] \tag{13}$$

where ν_L denotes the relevant *lattice* frequency (in general, x dependent) in the *absence* of Frenkel disorder and ν_i ($\neq \nu_L$) is the frequency of an interstitial oxygen (O_i). ν_L^i and ν_L^v, on the other hand, are the *perturbed* frequencies of n^i and n^v *regular* lattice ions which are nearest neighbors to O_i and V_L^0, respectively. (In the case of O_L nearest neighbors, $n^i = 8$ and $n^v = 6$.)

The onset at high temperature of (intrinsic) Frenkel disorder in a material ($UO_{2\pm x}$) with a *preexisting* degree of nonstoichiometry (x) suggests the following forms for ν_L^i and ν_L^v (in which the γ factors are possibly weakly x dependent):

$$\nu_L^i \simeq \nu_L(x)[1 + \gamma^i n], \qquad \nu_L^v \simeq \nu_L(x)[1 + \gamma^v n] \tag{14}$$

whence ΔS_{nc} assumes the form (provided $\gamma^i n$, $\gamma^v n \ll 1$)

$$\Delta S_{nc} = A(x) - Bn \tag{15}$$

where

$$A(x) = k \ln\left(\frac{\nu_L(x)}{\nu_i}\right), \qquad B \equiv (n^i\gamma^i + n^v\gamma^v)k$$

In order that Eq. (15) have the required form [Eq. (12)], it is thus necessary that

(i) the x dependence of $A(x)$ be negligible, and that $v_L(x) > v_i$; and

(ii) $B < 0$—consistent with the frequency perturbations induced in the vicinity of O_i and V_L^0 being of *opposite* signs (which is physically reasonable).

Since the above considerations are equally applicable to $UO_{2\pm x}$, we shall adopt the following Ansatz for $\Delta S_{nc}(x)$:

$$\Delta S_{nc}(x) = \Delta S_0^+ \pm \mu^{\pm} n(x) \tag{16}$$

where $\pm$ refers systematically to $UO_{2\pm x}$, and where $\Delta S_0^{\pm}$ and $\mu^{\pm}$ are constants, which—consistent with the hypothesis that at $x = 0$ the transition is of second order—must satisfy

$$\Delta S_0^- + \mu^- n(x=0) = \Delta S_c(x=0) = \Delta S_0^+ + \mu^+ n(x=0)$$

We now demonstrate that this Ansatz [Eq. (16)] is consistent with the experimental findings—namely, a second-order, λ-like, heat capacity peak in UO_2, which (as indicated by the presence of undercooling in the cooling curves; see Fig. 7) is converted into a first-order phase transition in UO_{2-x} [the temperature of which *increases* with x *above* the value $T_c(x=0)$ and which, in UO_{2+x}, is suppressed].

Consider first the case of stoichiometric $UO_{2.00}$. The realization of a second-order phase transition at a temperature T_c requires that, in addition to Eq. (10), the following conditions hold:

$$\left(\frac{\partial^2 F}{\partial n^2}\right) = 0, \qquad \left(\frac{\partial^3 F}{\partial n^3}\right) = 0, \qquad \left(\frac{\partial^4 F}{\partial n^4}\right) > 0 \tag{17}$$

In consequence of the admitted n dependence of F, $\partial^3 F/\partial n^3 = 0$ yields the defect concentration, n_c, at the critical temperature, T_c, the value of n_c being *independent* of w and λ and determined *solely* by the n dependence of S_{conf}. In turn, $(\partial^2 F/\partial n^2)_{n_c} = 0$ yields T_c in terms of λ, while $(\partial F/\partial n)_{n_c, T_c} = 0$ specifies (in terms of n_c, T_c, w, and λ) the value, ΔS_c, of ΔS_{nc} necessary for the realization of a second-order (critical-point) transition.

With the n dependences of the blocking factors α and β given by Eqs. (7) and (8), the results for Eq. (17) are shown in Fig. 11, at both $T = T_c$ and $T \gtrless T_c$; $\partial^3 F/\partial n^3 = 0$, yields $n_c \simeq 0.13$—a value which is consistent with the maximum (saturation) value indicated by the high-temperature neutron diffraction experiments [4]. Furthermore, it should be noted that this calculated value of n_c is relatively *in*sensitive to β

(consistent with the total number of sites available to V_L^0 being *twice* that available to O_i in the absence of blocking).

Since for nominally stoichiometry $UO_{2.00}$ the value of T_c is already *known* from experiment, $(\partial^2 F/\partial n^2)_{n_c} = 0$ gives the value of the energy λ which parameterizes the adopted "mean-field" treatment of the attractive vacancy–interstitial interaction [Eq. (4)]; taking $T_c(x=0) = 2670$ K, $(\partial^2 F/\partial n^2)_{n_c} = 0$ yields

$$\lambda = 2.74 \text{ eV} \qquad (\equiv \lambda_c) \tag{18}$$

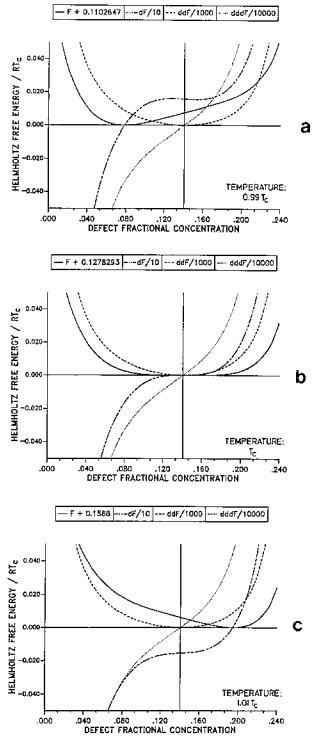

Fig. 11. Free energy (F) and its first (dF), second (ddF), and third (dddF) derivatives, as calculated from the assumed model: (a) at a temperature 1% below T_c; (b) at the critical temperature, T_c; and (c) at a temperature 1% above T_c. The rapid (but continuous) shift of the free energy minimum from low defect concentrations to high defect concentrations across T_c can be observed.

Finally, to satisfy $(\partial F/\partial n)_{n_c, T_c} = 0$, when $w = 3.67$ eV (the value inferred from coherent diffuse neutron scattering data [16] at $T \ll T_c$—and which is in good agreement with oxygen diffusion data [11] on UO_{2+x} in the limit $x \to 0$) requires that

$$\Delta S_c/k = 12.80 \tag{19}$$

Since this value just falls within the band of (Arrhenius) values $(5.5 \leqslant \Delta S/k \leqslant 12.8)$ obtained [11] at $T \ll T_c$, the consistency of our interpretation of the transition in stoichiometric $UO_{2.00}$ is upheld.

Furthermore, with these values of w, λ, and ΔS_c, the solutions, $\bar{n}(T)$, of $\partial F/\partial n = 0$ at arbitrary T, exhibit a *vertical* inflexion point at $T = T_c$—which, via Eq. (11), entails there a *divergent* λ-like C_v peak, which closely approximates to the observed C_p peak—while between T_c and T_m, $\bar{n}(T)$ increases from 0.13 to 0.21.

Let us now turn to consider the predictions of our model away from stoichiometry $(x \neq 0)$. This is most simply achieved by utilizing, as a reference, the extension of the above treatment of the second-order transition to $x \neq 0$, noting that within the adopted mean-field model the *vertical* inflexion point in $\bar{n}(T)$ at $T = T_c$ is to be regarded as the *vestigial remnant* of the *finite* (vertical) discontinuity which characterizes a *first*-order phase transition—the occurrence of which is promoted by an *increase* in the values of λ and/or ΔS_{nc} above those $(\lambda_c, \Delta S_c)$ required for a second-order transition. Any *decrease* below these values, on the other hand, suppresses the second-order transition—the associated λ-like singularity being replaced by a *finite* C_v peak[5] originating from a *non*vertical inflexion structure in $\bar{n}(T)$.

In our model, however, the only variable parameter is ΔS_{nc}, via the x dependence of Eq. (12) (in which n is x dependent), which, it should be noted, is significantly *weaker* than the (physically unrealistically) strong dependence required to maintain a second-order transition at $x \neq 0$. This is clear from Fig. 12, which summarizes the results obtained when the above treatment of the stoichiometric second-order transition is extended to $x \neq 0$, assuming that the values of w and λ retain their $x = 0$ values. The solution of $(\partial^2 F/\partial n^2)_{n_c} = 0$ then yields $T_c(x)$, while $(\partial F/\partial n)_{n_c, T_c} = 0$ determines the *formal* x dependence of $\partial S_{nc}/\partial n$ $[\equiv \Delta S_c(x)]$ necessary for the realization of a second-order transition at $x \neq 0$ $[\Delta S_c(x)$ is, of course, to be distinguished from the Ansatz given by Eq. (12)].

[5] Such finite peaks are sometimes claimed to be associated with so-called "diffuse" transitions—a terminology which we adopt, although it must be stressed that such "transitions" are not necessarily *phase* transitions.

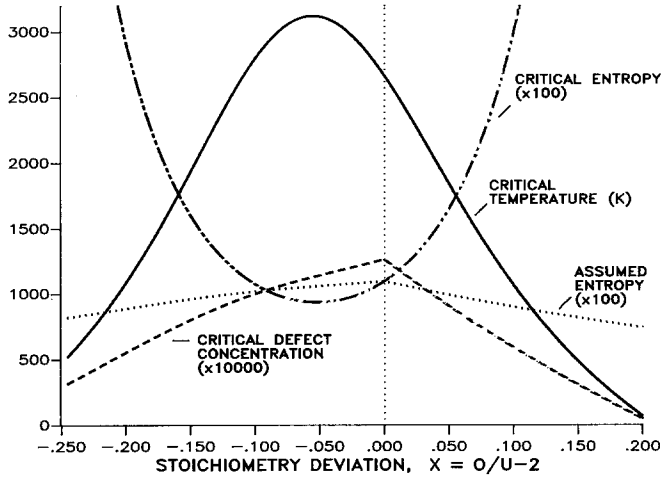

Fig. 12. Critical parameters for second-order transitions in $UO_{2\pm x}$.

In terms of Fig. 12 the differing behaviors of $UO_{2\pm x}$ are readily understandable. The nonsymmetrical disposition of $\Delta S_c(x)$ about $x=0$ *facilitates* the following inequalities:

$$\Delta S_{nc}[n_c(x)] > \Delta S_c(x) \quad \text{for} \quad UO_{2-x} \tag{20}$$

$$\Delta S_{nc}[n_c(x)] < \Delta S_c(x) \quad \text{for} \quad UO_{2+x} \tag{21}$$

where $\Delta S_{nc}[n_c(x)]$ is given by Eq. (12), with $n=n_c(x)$.

Provided that the value of μ^- is such that the inequality given in Eq. (20) is actually *realized*, it follows from the foregoing considerations that in UO_{2-x} there is a range of x over which the transition becomes first order—the temperature of which, $T_1(x)$, *increases* with x over the somewhat *smaller* range of x for which $\{\Delta S_{nc}[n_c(x)] - \Delta S_c(x)\}$ itself continues to increase with x. Requiring that the calculated values of $T_1(x)$ agree with the experimental values which increase monotonically with temperature, permits μ^- to be evaluated:

$$\mu^-/k = 27.9 \pm 2.8 \tag{22}$$

The results obtained for $C_v(UO_{2-x})$ are shown in Fig. 13; the corresponding transition temperatures are given in Table III.

In the case of UO_{2+x}, on the other hand, the value of μ^+ necessary for the realization of Eq. (21) could be similarly empirically determined if

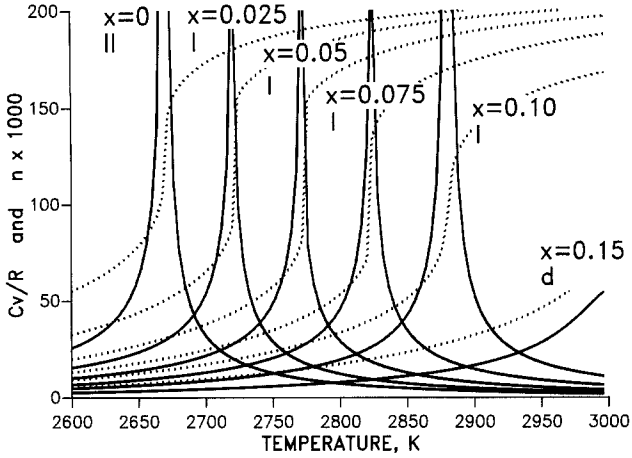

Fig. 13. Calculated C_v peaks at different stoichiometries in UO_{2-x}; the corresponding defect equilibrium concentrations n are indicated by the dotted curves; I, II, and d denote, respectively, first order, second order, and diffuse transitions.

the stoichiometry of the sample of UO_{2+x} with the *smallest* x value ($x = x_0$) which exhibits *no* C_p peak was known. For provided that the following inequality holds, Eq. (21) is satisfied for all x:

$$\frac{d}{dx}\Delta S_c(x)\bigg|_{x=0} > \frac{d}{dx}\Delta S_{nc}[n_c(x)]\bigg|_{x=0} \tag{23}$$

Table III. Calculated Premelting Transition Temperatures in UO_{2-x} [Assuming $T_c(x=0) = 2670$ K], Together with Details of the C_v Peak Associated with the Diffuse Transitions in UO_{2+x}

Transition type	Stoichiometry ×1000	Peak temperature (K)	Peak C_v (R)	50% peak width (K)
Diffuse	−150	3006	57	100
1st order	−100	2880	·	·
1st order	−75	2824	·	·
1st order	−50	2772	·	·
1st order	−25	2720	·	·
2nd order	0	2670	·	·
Diffuse	25	2746	180	30
Diffuse	50	2823	70	100
Diffuse	100	2963	20	350
Diffuse	150	3072	7	600

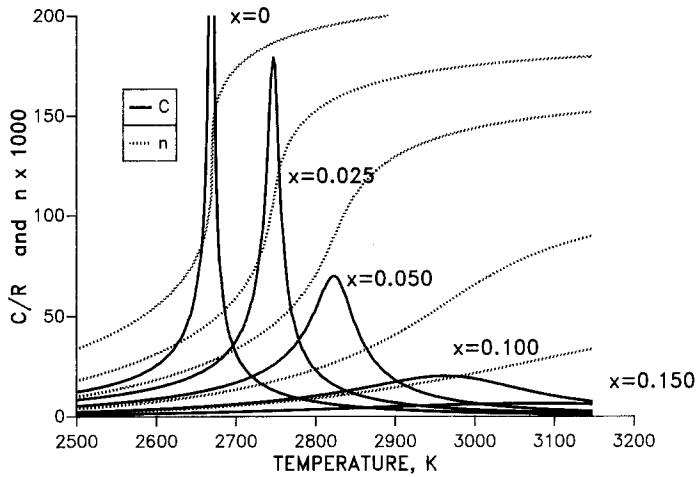

Fig. 14. Displacements of the C_v peak with stoichiometry in hyperstoichiometric UO_{2+x}. For $x > 0.25$ the peak temperatures reach and exceed the estimated melting line.

The strong monotonic increase in the difference $\{\Delta S_c(x) - \Delta S_{nc}[n_c(x)]\}$ then entails a correspondingly strong *suppression* of the associated C_v peak, so permitting μ^+ to be evaluated simply by requiring that at $x = x_0$, μ^+ be such as to effectively suppress any C_v peak.

The results for $C_v(UO_{2+x})$, obtained by assuming $\mu^+ = \mu^-$ [when μ^-/k is given by Eq. (22)], are shown in Fig. 14 and given quantitatively in Table III. It is shown that C_v peaks diminish very strongly with increasing x—the associated peak temperatures increasing toward the melting line (as adumbrated by Bredig [1]).

Thus the Ansatz

$$\Delta S_{nc}(x) = \Delta S_0^{\pm} + \mu^{\pm} n \tag{24}$$

not only reproduces the experimental trend in the case of UO_{2-x}, but also facilitates the suppression of the C_v peak in UO_{2+x}.

4. IMPLICATIONS FOR THE URANIA PHASE DIAGRAM

The experimental observation of λ-transitions in $UO_{2.00}$ and UO_{2-x}, together with the theoretical interpretation presented above, suggests some necessary refinements of the existing phase diagram of the material—although, given the uncertainty concerning the degree of nonstoichiometry of the various samples used our experiments, it is difficult to make quantitative recommendations. *Qualitatively*, however, the following is clear.

1. The $(x-T)$ phase field of UO_{2-x} must be divided by a line (indicated by T_t) of *first-order phase transitions* which starts at $T=2670$ K for $x=0$ and subsequently rises toward the *solidus* with increasing x, as shown in Fig. 15.
2. Although no λ-transition was detected in the case of the samples of UO_{2+x} (of undetermined stoichiometry) used in our experiments, it is interesting—and possibly physically significant—to note that for $x \neq 0$ the line $[T_c(x)]$ of *calculated* second-order λ-transitions decreases with increasing x from $T \equiv 2670$ K at $x=0$ and crosses the U_4O_9 phase boundary at a point near $T=700°C$, where a diffuse order–disorder transition is observed [17] in the oxygen superlattice—suggesting that the second-order λ-transition in $UO_{2.00}$ (involving disorder in the oxygen lattice) is the stoichiometric counterpart of this interstitial superlattice transition in U_4O_9. Above this line lies the locus of the temperatures of the *diffuse transitions actually predicted* for UO_{2+x} by our model—the experimental *absence* of any such associated peaks in our experiments under oxidizing conditions being consistent with the *calculated*[6] rapid decrease (increase) in peak height (width), provided that the x value of the sample is sufficiently large. The line of diffuse transitions (indicated by T_t) is shown as a dashed

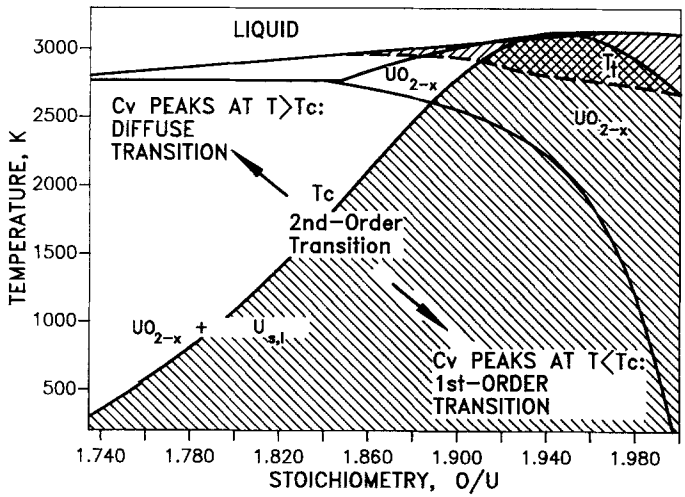

Fig. 15. Phase diagram of UO_{2-x}. The second-order transition temperature displays a maximum at $x=1.95$. The melting curve of UO_{2-x} is, *experimentally*, much better established than is that of UO_{2+x}.

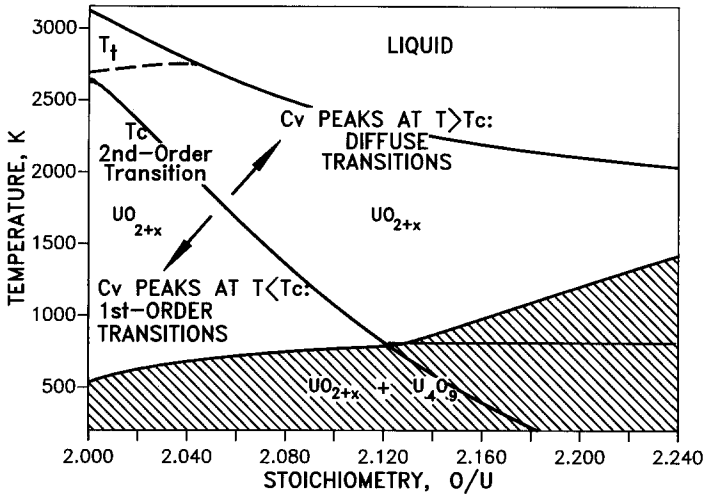

Fig. 16. Phase diagram of UO_{2+x}. The second-order transition temperature, $T_c(x)$, is a discriminating line in the phase field. Above T_c, order–disorder transitions in the oxygen sublattice are of the diffuse type, while below T_c they are first-order transitions. Note that the $T_c(x)$ line intersects the $UO_{2+x} + U_4O_9$ phase boundary at its inflexion point, defining a domain where continuous order–disorder transitions in U_4O_9 are actually observed a temperatures as low as 750 K; the locus of the diffuse transitions is shown as a dashed line (T_t).

line in Fig. 16, the calculated width and height of the corresponding peaks being given in Table III.

5. SUMMARY

The existence of a premelting transition $UO_{2.00}$ and UO_{2-x} has been confirmed by thermal analysis of the cooling curves of small, spherical samples of these materials, initially laser heated (on a subsecond time scale) to temperatures just below melting; in the UO_{2+x}, on the other hand, no such transition is detected. It is demonstrated that it is possible to understand the observed behavior in terms of a simple model based on anion Frenkel disorder, which is rendered a *cooperative process* by an attractive interaction between complementary (oppositely "charged") defects—the interstitials and vacancies. Crucial to the success of this program is the introduction of an (implicit) dependence of the nonconfigurational entropy, ΔS_{nc}, on the degree of nonstoichiometry, via its dependence on the concen-

[6] It may be noted that a similar behavior is found *experimentally* in $Pb_{1-y}U_yF_{2+2y}$, where the C_p peak essentially vanishes [18] for $y > 0.1$.

tration, n, of intrinsic Frenkel defects in $UO_{2\pm x}$; unfortunately, however, only plausibility arguments can, at present, be given in support of the admitted *linear* dependence.

In connection with the implications of our analysis on the phase diagram of the U–O system, on the other hand, it is particularly interesting to note that the calculated (but unrealized) line of second-order phase transitions, $T_c(x)$, in UO_{2+x} (which, of course, is quite *independent* of the admitted linear dependence of ΔS_{nc} on n) intersects the UO_{2+x}–U_4O_9 phase boundary near to where a high-temperature diffuse order–disorder transition has been observed in the oxygen superlattice, suggesting that the second-order, λ-transition in $UO_{2.00}$ is the stoichiometric counterpart of this transition U_4O_9.

Finally, the empirical confirmation of a Bredig transition in UO_2 necessitates a revision of existing analyses (e.g., Refs. 19 and 20) of the *total* heat capacity of the material into its constituent contributions; this—together with a detailed consideration of the $C_p - C_v$ difference—will be presented in a future publication.

REFERENCES

1. M. A. Bredig, Oak Ridge National Laboratory, Report 4437 (1969), p. 103.
2. R. A. Hein and P. N. Flagella, GEMP-578 (General Electric Company, Schenectady, NY, 1968).
3. J. Ralph and G. J. Hyland, *J. Nucl. Math.* **132**:76 (1985).
4. M. T. Hutchings, *J. Chem. Soc. Faraday Trans II* **83**:1083 (1987).
5. M. T. Hutchings, K. Clausen, M. H. Dickens, W. Hayes, J. K. Kjems, P. G. Schnabel, and C. Smith, *J. Phys. C* **17**:3903 (1984).
6. C. E. Derrington, A. Lindner, and M. O'Keeffe, *J. Sol. State Chem.* **15**:171 (1975).
7. W. Schröter and J. Nölting, *J. Phys. Colloq.* **C6**(41):20 (1980).
8. J. P. Hiernaut, F. Sakuma, and C. Ronchi, *High Temp. High Press.* **21**:139 (1989).
9. J. P. Hiernaut and C. Ronchi, *High Temp. High Press.* **21**:119 (1989).
10. C. R. A. Catlow, J. D. Comins, F. A. Germano, R. T. Harley, and W. Hayes, *J. Phys. C* **11**:3197 (1978).
11. K. C. Kim and D. R. Olander, *J. Nucl. Mat.* **102**:192 (1981).
12. R. Speiser and J. W. Spretnak, *Trans AIME* **47**:493 (1955).
13. K. Hagemark and M. Broli, *J. Nucl. Inorg. Chem.* **28**:2837 (1966).
14. R. J. Thorn and G. H. Winslow, *J. Chem. Phys.* **44**:2632 (1966) (in particular, see Appendix, p. 2643).
15. N. F. Mott and R. W. Gurney, *Electronic Processes in Ionic Crystals* (Dover, New York, 1964), pp. 31–32.
16. K. N. Clausen, M. A. Hackett, W. Hayes, S. Hull, M. T. Hutchings, J. E. MacDonald, K. A. McEwen, R. Osborn, and U. Steigenberger, *Physica B* **156, 157**:103 (1989).
17. H. Blank and C. Ronchi, *Acta Cryst.* **A24**:657 (1968).
18. N. Hessel Andersen, K. Clausen, and J. K. Kjems, *Sol. State Ionics* **9, 10**:543 (1983).
19. P. Browning, G. J. Hyland, and J. Ralph, *High Temp. High Press.* **15**:169 (1983).
20. G. J. Hyland and J. Ralph, *High Temp. High Press.* **17**:653 (1985).